Numerical Analysis of Plume Characteristics and Liquid Circulation in Gas Injection Through a Porous Plug

Choeng Ryul Choi*
Mechanical Engineering Department, Graduate School of Kyunghee University
Chang Nyung Kim
College of Mechanical & Industrial System Engineering, Kyunghee University

Two phase flows have been numerically calculated to analyze plume characteristics and liquid circulation in gas injection through a porous plug. The Eulerian approach has been used for formulation of both the continuous and dispersed phases. The turbulence in the liquid phase has been modeled using the standard k-ε turbulence model. The interphase friction coefficient has been calculated using correlations available in the literature. The turbulent dispersion of the phases has been modeled by the "dispersion Prandtl number". The predicted mean flows is compared well with the experimental data. The plume region area and the axial velocities are increased with the gas flow rate and with the decrease in the inlet area. The turbulent intensity also shows the same trend. Also, the space-averaged turbulent kinetic energy for various gas flow rates and inlet areas has been obtained. The results are of interest in the design and operation of a wide variety of materials and chemical processing operations.

Key Words : Gas Injection System, Ladle, Two-Phase, Eulerian Approach, Interphase Friction Coefficient, Plume

Nomenclature

C_d : Dimensionless drag coefficient
C_f : Interphase fricti on coefficient
d_b : Bubble diameter
D_t : Phase dispersion coefficient
$\vec{F}$: Interfacial force per unit volume
g : Gravity force
H : Height of vessel
k : Turbulent kinetic energy
p : Pressure
Q : Gas flow rate
r : Radial distance
r^* : Dimensionless radial distance
R : Volume fraction or radius of vessel
Re : Bubble Reynolds number
v : Radial velocity component
V_c : Volume of cell
V_r : Relative velocity
w : Axial velocity component
z : Axial distance
z^* : Dimensionless axial distance

Greek Letters

ε : Dissipation rate
μ : Viscosity
ν : Kinetic viscosity
ρ : Density
σ : Dispersion Prandtl number
ϕ : k or ε

Subscripts

g : Gas phase
i : Gas or Liquid phase
l : Liquid phase
t : Turbulence

* Corresponding Author,
E-mail : crchoi@cvs2.kyunghee.ac.kr
TEL : +82-31-201-2869 ; **FAX** : +82-31-202-8106
Mechanical Engineering Department, Graduate School of Kyunghee University, 1 Seochon, Kihung, Yongin 449-701, Korea. (Manuscript **Received** August 23, 1999; **Revised** January 19, 2000)

1. Introduction

In the metallurgical and chemical process industries, there are many processes where liquid phase contained in a vessel is stirred with injection of a gas phase through porous plug situated at the base of the ladle for generation of a turbulent recirculating flow. The injected gas rises through the liquid due to buoyancy and leaves the free surface at the top, as shown in Fig. 1. The interaction of momentum transfer involved in the liquid and gas phases induces a conical recirculation zone. The gas rising through the liquid performs converting energy, refining melts, mixing contents, enhancing chemical reaction rate, removing particles, and homogenizing temperature and chemical composition. In addition, it may prevent agglomerating inclusion that causes a decrease of the quality of final product. Usually, for reduction of the inclusion, it is necessary to obtain a large contact area between the phases and to avoid dead water regions.

Despite these popularity, however, the design of gas injection systems is currently based on trial and error methods and would be greatly enhanced by a better understanding of underlying fluid dynamics. Several techniques have been used to investigate the nature of flows in two-phase region. A numerical two-phase model has been developed to predict the transport processes in the gas injection systems. A number of workers investigated the structure of two phase bubbly flows found in gas injection systems. Such models are based on the force balance between the liquid inertia and the combination of buoyancy and friction forces on the gas.

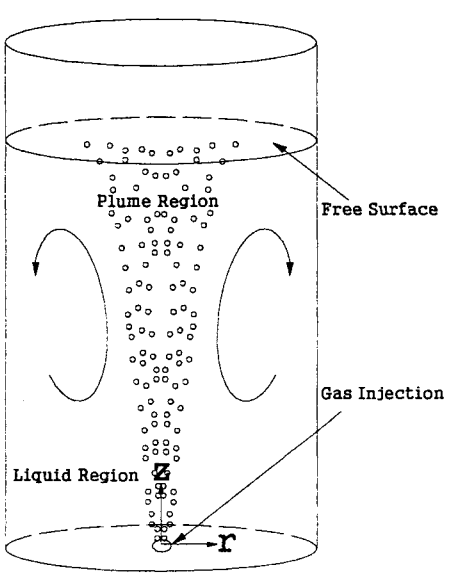

Fig. 1 Configuration of the gas injection system

Szekely and Asai(1975) were among the first to model the bubble driven flows in gas injection systems. They used the k-ε turbulence model and assumed that the bubbles were contained in a cylindrical region of a given diameter. A better handling of the bubbly phase was suggested by Debroy et al.(1978). They used a quasi single phase calculation procedure to simulate the plume region, introducing two void fraction expressions (no-slip case as well as slip case), and using a single valued effective viscosity. Sahai and Guthrie(1982) and Oinglin et al.(1984) developed more elaborate models based on the k-ε turbulence model with the existing quasi single phase calculation procedure. Grevet et al.(1982) conducted the experiments using a laser Doppler anemometer to measure rms velocity components. Mckelliget et al.(1982) investigated the vertical and horizontal injection cases. The gas-liquid mixture was treated as a continuous fluid of various densities. Cross et al.(1984) studied the problem of the gas injections by solving the transport equations for both the liquid and gas phases in a Eulerian reference frame. Mazumdar and Guthrie(1985) compared the mean velocity predictions of the k-ε turbulence model and another simpler model such as the bulk effective viscosity model. Koh et al.(1987) developed a considerably different approach. The gas and liquid phases were considered as two different fields interpenetrating and interacting with each other. The problem was formulated on the basis of the mass, momentum, and energy transports between the phases sharing the same space. Johansen et al. (1988) conducted a very elaborate experiment using a laser Doppler anemometer to measure velocity components and to investigate dispersion phenomena in the two phase region. Johansen

and Boysan(1988) first introduced the Lagrangian-Eulerian approach.

Recently, the Lagrangian-Eulerian approach was adapted by Mazumdar and Guthrie(1994) and Neifer et al. (1993) in model analysis.

The overall purpose of the present study is to investigate two phase flow characteristics in a submerged gas injection system. This study has been carried out for the better understanding of the physics involved in complex systems including two-phase flows, and the results are also expected to be of direct use in the efficient and optimal design of gas injection systems. First, the results obtained in the present calculations has been compared with the experimental data of Johansen et al. (1988) to prove the propriety of the applied mathematical model. The geometry and injection parameters considered are identical to those studied by them. Secondarily, the calculations have been performed and compared for various gas flow rate and inlet area to investigate the effects of both gas flow rate and inlet area on the entire flow field phenomena and the dispersion rate of the plume.

2. Mathematical Formulation

The gas injection system includes a two phase turbulent recirculating flow. There are relative motions involved between the phases together with interchange of the momentum. Thus, the governing equations should reflect these interactions between the phases. The problem has been formulated on the basis of a two-fluid model using the Eulerian approach for both phases.

This formulation assumes that both phases may exist in the same computational cell at the same time, and that each phase consists of a continuous field interpenetrating and interacting with the other in the domain. Any small volume of space in interesting region at any time can be regarded as containing a volume fraction, α_i, of the i phase, so that

$$\alpha_l+\alpha_g=1 \tag{1}$$

The subscripts l and g denote the liquid and the gas phase, respectively.

The standard k-ε turbulence model has been applied for the liquid phase only. Since compared with the liquid phase, the gas phase has quite low density and momentum, no turbulence model has been applied for the gas phase. Specifying an effective turbulent viscosity for the gas phase has little effect on the overall predictions.

2.1 Governing equations

The flow is axisymmetric, steady and turbulent. The local pressure is common for both phases and no mass is transferred between the phases. The momentum exchange is made through exchange terms in momentum. With above assumptions, the differential equations governing the process can be written as follows.

◎ Mass conservation equations

Liquid phase mass conservation equation

$$\frac{1}{r}\frac{\partial}{\partial r}(r\alpha_l\rho_l v_l)+\frac{\partial}{\partial z}(\alpha_l\rho_l w_l) -\mathrm{div}(\rho_l D_{t,l}\,\mathrm{grad}\,\alpha_l)=0 \tag{2}$$

Gas phase mass conservation equation

$$\frac{1}{r}\frac{\partial}{\partial r}(r\alpha_g\rho_g v_g)+\frac{\partial}{\partial z}(\alpha_g\rho_g w_g) -\mathrm{div}(\rho_g D_{t,g}\,\mathrm{grad}\,\alpha_g)=0 \tag{3}$$

where the last term on the left-hand side of each mass conservation equation represents the turbulent dispersion of the liquid and gas phases, respectively, by random motion mechanisms.

D_t is the phase diffusion coefficient.

$$D_{t,i}=\rho_i\left(\frac{\nu_l}{\sigma_{l,i}}+\frac{\nu_t}{\sigma_{t,i}}\right) \tag{4}$$

where the subscript i denotes either the gas or the liquid phase. ν_l, ν_t, σ_l, and σ_t represent the laminar kinematic viscosity of the liquid phase, the turbulent kinematic viscosity of the liquid phase, the laminar dispersion Prandtl number(in present calculations, $\sigma_l=10^{10}$), and the turbulent dispersion Prandtl number(in present calculations, $\sigma_t=1.0$), respectively.

◎ Momentum conservation equations

Liquid phase momentum equation in the radial direction

$$\frac{1}{r}\frac{\partial}{\partial r}(\alpha_l\rho_l r\, v_l^2)+\frac{\partial}{\partial z}(\alpha_l\rho_l w_l v_l)$$
$$=-\alpha_l\frac{\partial p}{\partial r}+\frac{2}{r}\frac{\partial}{\partial r}\left(\alpha_l r\mu_{eff,l}\frac{\partial v_l}{\partial r}\right)$$
$$+\frac{\partial}{\partial z}\left(\alpha_l\mu_{eff,l}\frac{\partial v_l}{\partial z}\right)+\frac{\partial}{\partial z}\left(\alpha_l\mu_{eff,l}\frac{\partial w_l}{\partial z}\right)$$
$$-\frac{2\alpha_l v_l\mu_{eff,l}}{r^2}+C_f(v_g-v_l) \tag{5}$$

Gas phase momentum equation in the radial direction

$$\frac{1}{r}\frac{\partial}{\partial r}(\alpha_g\rho_g r\, v_g^2)+\frac{\partial}{\partial z}(\alpha_g\rho_g w_g v_g)$$
$$=-\alpha_g\frac{\partial p}{\partial r}+\frac{2}{r}\frac{\partial}{\partial r}\left(\alpha_g r\mu_{eff,g}\frac{\partial v_g}{\partial r}\right)$$
$$+\frac{\partial}{\partial z}\left(\alpha_g\mu_{eff,g}\frac{\partial v_g}{\partial z}\right)+\frac{\partial}{\partial z}\left(\alpha_g\mu_{eff,g}\frac{\partial w_g}{\partial z}\right)$$
$$-\frac{2\alpha_g v_g\mu_{eff,g}}{r^2}+C_f(v_l-v_g) \tag{6}$$

Liquid phase momentum equation in the axial direction

$$\frac{1}{r}\frac{\partial}{\partial r}(\alpha_l\rho_l r v_l w_l^2)+\frac{\partial}{\partial z}(\alpha_l\rho_l w_l^2)$$
$$=-\alpha_l\frac{\partial p}{\partial r}+\frac{1}{r}\frac{\partial}{\partial r}\left(\alpha_l r\mu_{eff,l}\frac{\partial w_l}{\partial r}\right)$$
$$+2\frac{\partial}{\partial z}\left(\alpha_l\mu_{eff,l}\frac{\partial w_l}{\partial z}\right)+\frac{\partial}{\partial z}\left(\alpha_l r\mu_{eff,l}\frac{\partial v_l}{\partial r}\right)$$
$$-\rho_l\alpha_l g+C_f(w_g-w_l) \tag{7}$$

Gas phase momentum equation in the axial direction

$$\frac{1}{r}\frac{\partial}{\partial r}(\alpha_g\rho_g r\, v_g w_g)+\frac{\partial}{\partial z}(\alpha_g\rho_g w_g^2)$$
$$=-\alpha_g\frac{\partial p}{\partial r}+\frac{1}{r}\frac{\partial}{\partial r}\left(\alpha_g r\mu_{eff,g}\frac{\partial w_g}{\partial r}\right)$$
$$+2\frac{\partial}{\partial z}\left(\alpha_g\mu_{eff,g}\frac{\partial w_g}{\partial z}\right)+\frac{1}{r}\frac{\partial}{\partial z}\left(\alpha_g\mu_{eff,g}\frac{\partial v_g}{\partial r}\right)$$
$$+\alpha_g\rho_g g+C_f(w_l-w_g) \tag{8}$$

where C_f is the interphase friction force per unit volume and per unit relative velocity. It is written as

$$C_f=\frac{3}{4}\frac{C_d\rho_l\alpha_g|\bar{V}_r|V_c}{d_b} \tag{9}$$

where C_d, $|\bar{V}_r|$, V_c, and d_b are the dimensionless drag coefficient, the velocity difference between phases, the cell volume, and the diameter of bubbles, respectively. The drag coefficient C_d is an empirically or semi-empirically determined parameter which differs from one flow regime to another. It is assumed that the flow regime is the dispersed flow for the present calculation. Also, it is assumed that the continuous phase is liquid and the dispersed phase is gas.

In the present calculation, the drag coefficient, D_d, has been calculated from the standard drag curve introduced by Clift et al. (1978).

① for $Re<3.38\times10^5$

$$C_d=\frac{24\cdot(1+0.15\cdot Re^{0.687})}{Re}+\frac{0.42}{1+\frac{42500}{Re^{1.16}}}$$

② for $3.38\times10^5<Re<4.0\times10^5$

$$C_d=29.78-(5.3\times\log_{10}Re)$$

③ for $4.0\times10^5<Re<1.0\times10^6$

$$C_d=0.1\times\log_{10}Re-0.49$$

④ for $1.0\times10^6<Re$

$$C_d=0.19-\frac{8.0\times10^4}{Re} \tag{10}$$

where

$$Re=\frac{|V_r|d_b}{\nu_l} \tag{11}$$

In the present calculation, the bubble size has been assumed to be uniform over the entire flow domain. But, this model can be improved in the near future to have capability to handle non uniform bubble size distribution if such information is available.

The effective viscosity, μ_{eff}, is calculated from

$$\mu_{eff,i}=\rho_l\left(\frac{\nu_l}{\sigma_{l,i}}+\frac{\nu_t}{\sigma_{t,i}}\right),\quad \nu_t=C_\mu\cdot\frac{k^2}{\varepsilon} \tag{12}$$

where σ_l and σ_t represent the laminar Prandtl number (in present calculations, $\sigma_l=1.0$) and the turbulent Prandtl number (in present calculations, $\sigma_t=1.0$), respectively.

◎ Conservation equations for the liquid phase turbulence kinetic energy, k, and its dissipation rate, ε

$$\frac{1}{r}\frac{\partial}{\partial r}(\alpha_l\rho_l r v_l\phi)+\frac{\partial}{\partial z}(\alpha_l\rho_l w_l\phi)$$
$$-\frac{\partial}{\partial z}\left(\frac{\alpha_l\mu_{eff}}{\sigma_\phi}\frac{\partial\phi}{\partial z}\right)-\frac{1}{r}\frac{\partial}{\partial r}\left(\alpha_l r\frac{\mu_{eff}}{\sigma_\phi}\frac{\partial\phi}{\partial z}\right)=S_\phi \tag{13}$$

where ϕ represents either k or ε. The source terms, S_ϕ, of k and ε are

$$S_k=\alpha_l(G_k-\rho_l\varepsilon) \tag{14}$$

$$S_\varepsilon=\alpha_l\frac{\varepsilon}{k}(C_1G_k-C_2\rho_l\varepsilon) \tag{15}$$

where

$$G_k=\mu_f\left\{2\left[\left(\frac{\partial w_l}{\partial z}\right)^2+\left(\frac{\partial v_l}{\partial r}\right)^2+\left(\frac{v_l}{r}\right)^2\right]+\left(\frac{\partial w_l}{\partial r}+\frac{\partial v_l}{\partial z}\right)^2\right\} \tag{16}$$

The above constants are assigned to have the same values as in the single phase flow. (C_μ=0.09, C_1=1.44, C_2=1.92, σ_k=1.0, σ_ε=1.3)

2.2 Boundary conditions

Boundary conditions are considered at the inlet and outlet, at the side and bottom walls and along the axis. At the inlet boundary, flat velocity has been assumed for the injected gas. The gas volume fraction, α_g, has been set to a value of unity, and the liquid volume fraction, α_l, zero.

At the outlet boundary, which is located at the top surface of the calculation domain, only the gas phase is allowed to leave the domain at the same rate as it arrives at the top. This condition is feasible by fixing the atmospheric pressure at the outlet boundary. The liquid phase is not allowed to leave the system, and the zero shear condition is applied for both phases.

$$w_l=0 \text{ and } \frac{\partial v_l}{\partial z}=\frac{\partial v_g}{\partial z}=\frac{\partial k}{\partial z}=\frac{\partial \varepsilon}{\partial z}=0 \tag{17}$$

Along the axis, symmetry conditions are applied as

$$v_l=v_g=0,\quad \frac{\partial w_l}{\partial r}=\frac{\partial w_g}{\partial r}=\frac{\partial k}{\partial r}=\frac{\partial \varepsilon}{\partial r}=0 \tag{18}$$

and

$$\frac{\partial \alpha_l}{\partial r}=\frac{\partial \alpha_g}{\partial r}=0 \tag{19}$$

At the side and the bottom walls, the no slip conditions are applied as

$$v_1=v_2=w_1=w_2=0 \tag{20}$$

The logarithmic law of wall is used to calculate the values of the k and ε (for the liquid phase) at the near wall points.

3. Numerical Solution Method

The governing equations have been changed to algebraic equations using a difference scheme on the basis of the control volume formulation of Patankar(1980). The finite difference equations have been derived using a hybrid differencing scheme over the staggered grid system. The pressure field is obtained by means of IPSA(Inter-Phase Slip Algorithm), which is a computational method that the pressure field is obtained from the composition of the volume fraction and the momentum equation in a two phase flow. The solution procedure is similar to SIMPLE algorithm(Patankar and Spalding, 1972) used in a single phase flow.

The IPSA solution procedure is then;

(1) Guess pressures.

(2) Solve volume fractions, using in-store velocities and volume fractions.

(3) Solve the momentum equations using the new volume fractions and guessed pressures.

(4) Construct the representative continuity errors by weighting and adding the phase continuity equations.

(5) Construct and solve the pressure correction equation.

(6) Apply corrections of pressure and all velocities.

(7) Repeat the procedure from the step (2) to the step (6) until convergence is met.

The equations for radial velocity components, turbulent kinetic energy, and its dissipation have been solved by the Jacobian point by point method. The vertical velocity components have been solved by a slab-wise simultaneous solver. The pressure correction equation has been solved by a whole field simultaneous solver.

4. Results and Discussion

In the present study, a vertical air injection into a cylindrical vessel containing water has been considered(Fig. 1). Instead of the gas-melt system, an air-water system has been chosen so that the results predicted in the present calculation

could be directly compared with the experimental data obtained by Johansen et al. (1988). The present model, however, is applicable to gas-liquid metal systems as well.

The physical system is the same as the configuration used by Johansen et al. (1988). It consists of a slightly conical perspex reactor with free surface. Its height is 1.237m and the top and bottom diameters are 1.10m and 0.93m, respectively. Air is injected through a centrally located 5 cm diameter porous plug. In the present calculation, ladle in Fig. 1 is assumed to be a cylindrical vessel of height(H) of 1.237m and radius(R) of 0.5m which is a reasonable approximation to the geometry of Johansen et al. (1988). With several preliminary calculations with different grid sizes, a 25×83 ($r\times z$) mesh system was chosen to be optimum for numerical accuracy and computational cost.

4.1 Bench marking of the present calculation

Calculation has been performed to prove the propriety of applied mathematical formulation. The air volume flow rate, Q, is 6.1×10^{-4} m^3/s, and the average bubble diameter used is 11.5mm evaluated from the following expression

$$d_b=0.35\ (Q^2/g)^{0.2} \tag{21}$$

which has been given by Davison and Sch ler (1960) and has been found to agree reasonably with the experimental observations by Johansen et al. (1988). The results predicted in the present calculation are directly compared with the experimental data.

The calculated velocity vector field is shown in Fig. 2(a). It can be seen that the flow exhibits a jet-like character in the vicinity of the symmetry axis with parabolic axial velocities. The jet is deflected sideways as it reaches the free surface due to static pressure resulting in redistribution of the velocity and turbulent kinetic energy(Fig. 2 (c)), giving rise to relatively large radial velocity components. Due to the continuity requirements, a toroidal recirculation zone is located in the upper corners of the vessel. In the bottom corner regions the flow appears to be almost stagnant

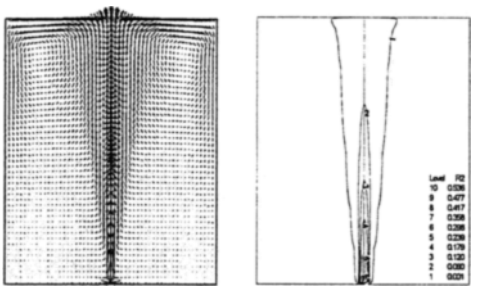

(a) Velocity of liquid (b) Volume fraction of gas

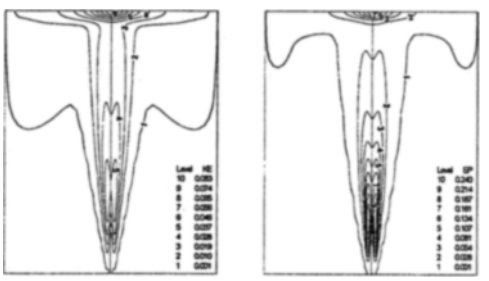

(c) Turbulent kinetic energy (d) Turbulent dissipation

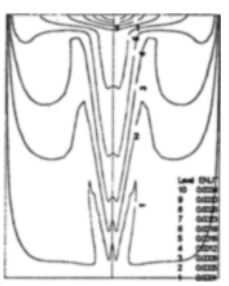

(e) Effective kinetic viscosity

Fig. 2 Calculated results for bench marking

implying poor mixing and high probability of particulate deposition.

The conical plume region is shown in Fig. 2 (b). A region with a high gas volume fraction is observed to be very close to the injection nozzle. As expected, when gas goes up, the gas volume fraction decreases with the increase in the total amount of the entrained liquid. In Figs. 2(c) and 2(d), the calculated turbulent kinetic energy, and its dissipation rate are shown, respectively. General tendency of the distributions are alike each other for the kinetic energy and dissipation rate. However, in the flow field each value is seen to be higher both in the jet cone region and near the free surface.

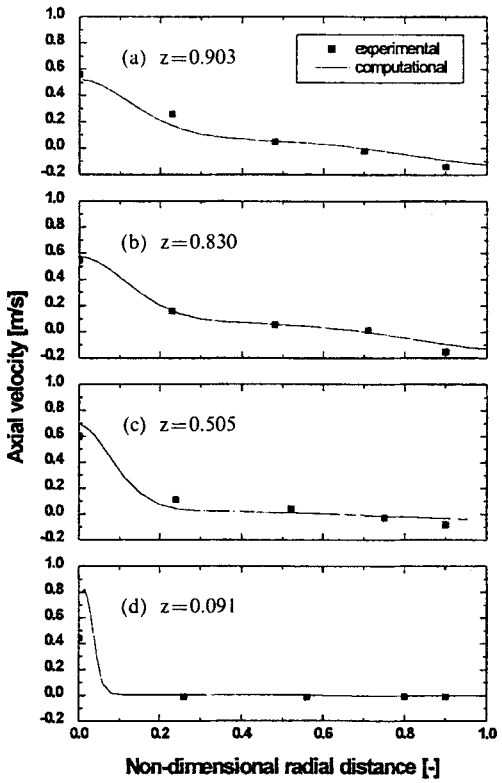

Fig. 3 Comparison of calculated and experimental axial velocities ($z^*=z/H$, $r^*=r/R$)

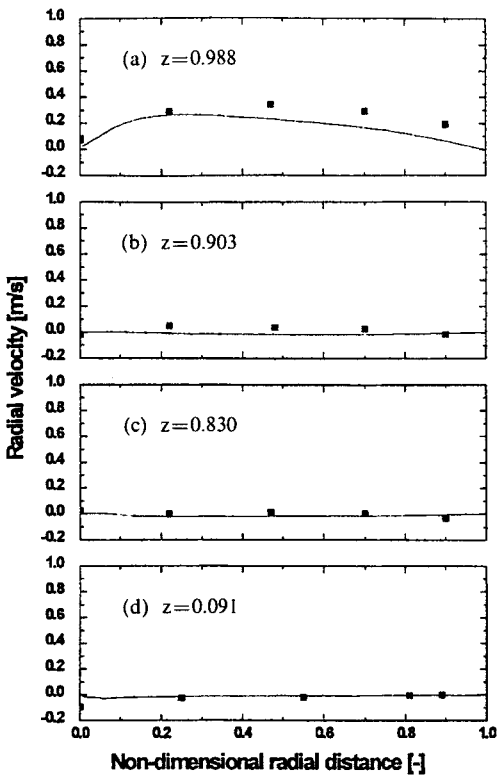

Fig. 4 Comparison of calculated and experimental radial velocities

The effective kinetic viscosity varies extensively over the whole flow field (Fig. 2(e)). This indicates that the assumption of uniform kinetic viscosity may not be appropriate. Comparisons of the calculated and experimental axial velocities along the radial position at various dimensionless axial heights are shown in Fig. 3. The calculated results agree well with the experimental results except at the lower region near injection plug (Fig. 3(d)). This discrepancy at the lower region may be attributed to the neglect of bubble breakup and coalescence in the region where the accurate information on these phenomena lacks, and to the assumption of the dispersed flow over the entire flow field.

Comparisons of calculated and experimental radial velocities along the radial direction at the various dimensionless axial heights are shown in Fig. 4. The calculated results agree reasonably with the experimental results except near the free surface. The predictions clearly show that a centrally placed porous plug leads to low velocities and poor mixing in the corner regions, which should be avoided in order to enhance composition homogenization.

4.2 Effects of gas injection flow rate

To analyze the effects of gas flow rate on the flow characteristics, calculations were performed for various gas injection volume flow rates, Q, (1.3, 3.3, 4.7, 6.1, 7.5×10^{-4} m^3/s) with bubble diameter 11.5 mm. The calculated velocity, gas volume fraction, and turbulent kinetic energy distribution are given in Fig. 5. Here, two cases are compared each other and the flow field with larger flow rate (right side) shows higher axial velocity, higher gas volume fraction and higher turbulence kinetic energy. In Fig. 6, the comparisons of the axial velocities for various gas volume flow rates along the radial position at different dimensionless axial heights are shown. The plume region grows wider and the centerline axial

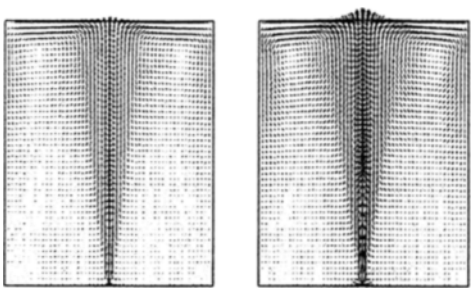

(a) Distribution of liquid velocity

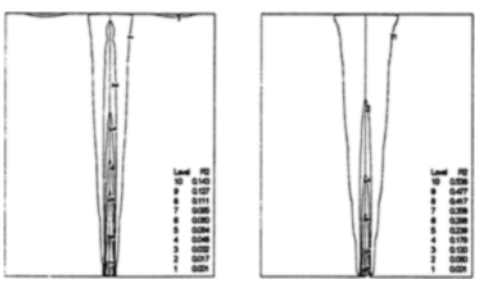

(b) Distribution of gas volume fraction

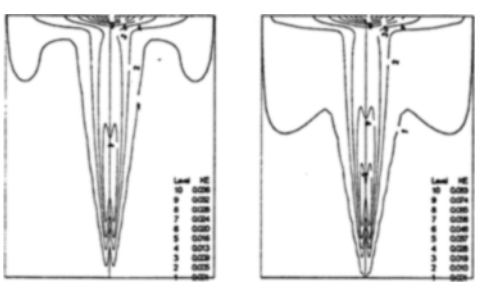

(c) Distribution of turbulence kinetic energy

Fig. 5 Effect of gas injection flow rate (left: 1.9×10^{-4} m^3/s, right: 6.1×10^{-4} m^3/s)

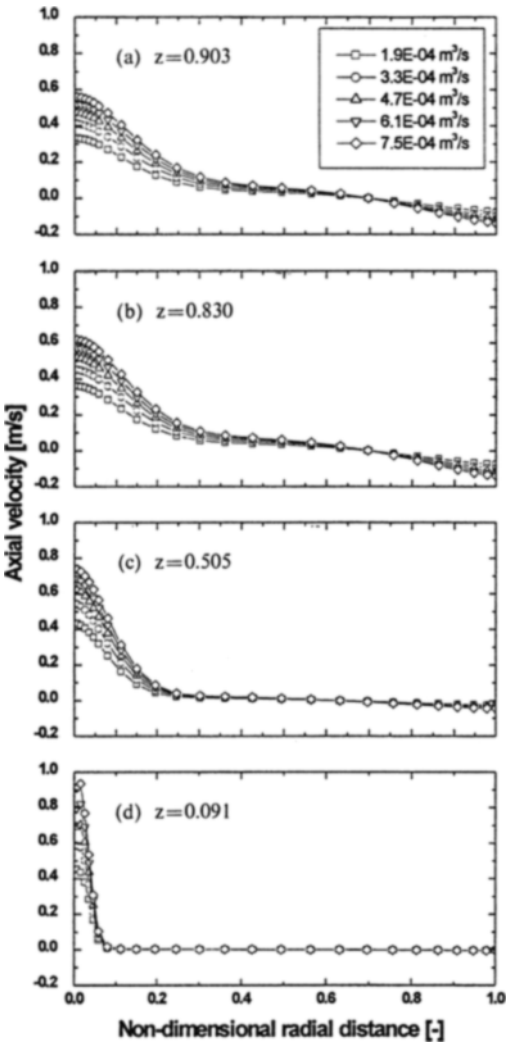

Fig. 6 Comparison of the axial velocities for various gas injection flow rates

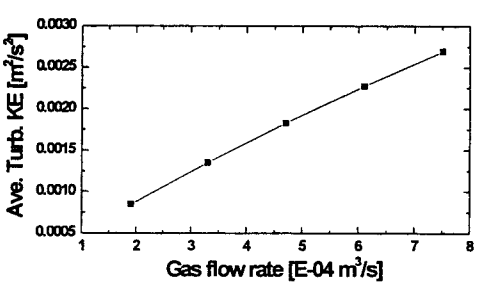

Fig. 7 Averaged turbulence kinetic energy for various gas injection flow rates

velocity is increased with the gas flow rate. This is due to a high interacting force between gas and liquid when gas flow rate is large.

The space-averaged turbulent kinetic energy for various gas flow rates is given in Fig. 7. The averaged turbulent kinetic energy seems to linearly increase as the gas flow rate increases in the range of the current calculation.

4.3 Effects of inlet area

Calculations were performed for various inlet areas (0.98, 1.96, 2.94, 3.93, 5.89×10^{-3} m^2) with an air volume flow rate, Q, 6.1×10^{-4} m^3/s. The calculated velocity, gas volume fraction, and turbulent kinetic energy distribution are shown in Fig. 8. In the current calculation, the case of inlet

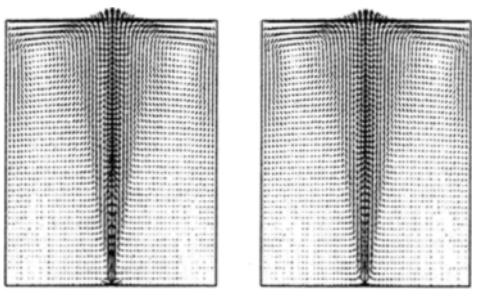

(a) Distribution of liquid velocity

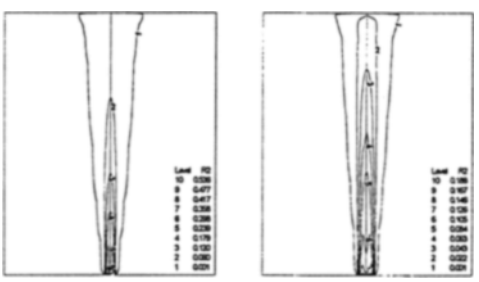

(b) Distribution of gas volume fraction

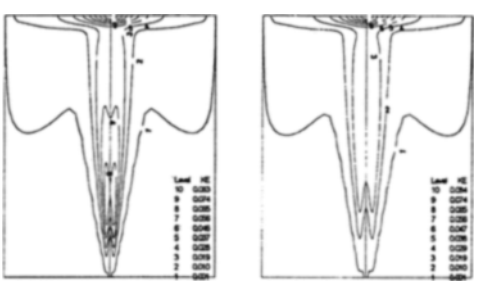

(c) Distribution of turbulence kinetic energy

Fig. 8 Effect of inlet area
(left: 1.96×10^{-3} m^2, right: 5.89×10^{-3} m^2)

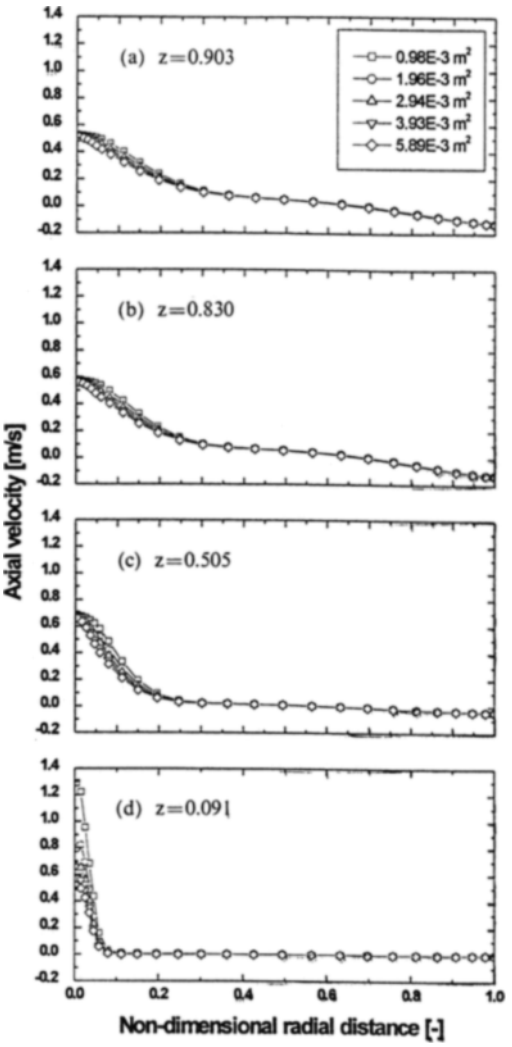

Fig. 9 Comparison of the axial velocities for various inlet areas

area 1.96×10^{-3} m^2 is identical to the case of a 5 cm diameter porous plug used for the bench marking of the present model before. It can be seen that both gas volume fraction and turbulent kinetic energy are smaller in the case of larger inlet area due to the spatially distributed injection of gas at the inlet. In Fig. 9, the comparison of the axial velocities for various inlet areas at different dimensionless axial heights is given. Except for the vicinity of the inlet, there is not considerable difference in the axial velocities between the flow fields with different inlet areas, only expressing a little bit smaller velocity with a larger inlet area. However, near the injection nozzle axial velocity with larger injection area is quite smaller.

The averaged turbulent kinetic energy is given in Fig. 10. The averaged turbulent kinetic energy almost logarithmically increases with the inlet area.

With reference to the various boundary conditions applied in the current hydrodynamic model, considerable idealizations have been applied in the vicinity of the liquid's free surface and the gas injection nozzle. In this model, the free surface has been assumed to be essentially flat. Therefore the presence of a spout, together with waves, has been ignored in the computation procedures.

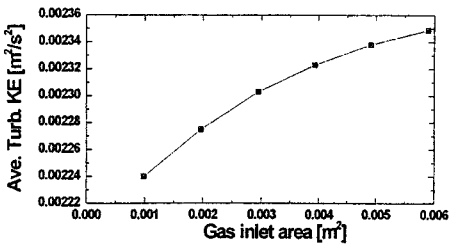

Fig. 10 Averaged turbulence kinetic energy for various inlet areas

In addition, for the two phase flow model, pure gas stream velocity has been applied as a inlet boundary condition for the gas flow momentum equation. According to Sahai et al. (1982), the gas injection into the liquid phase is accompanied by formation of a large bubble and a gas envelope over the nozzle tip, which tends to induce the hydrodynamic instability. Subsequently, the bubble or gas envelope shatters and breaks up into an array of small bubbles. However, from the metallurgical point of view, this phenomenon has little effect on the overall momentum and heat transfer in a ladle because the region where bubble breaking phenomena occur is only 4~5% of the total ladle size.

Mazumdar et al. (1990, 1992) have estimated the mass transfer coefficients for vertically submerged cylinders in a water model ladle and have proposed a following correlation:

$$Sh = 0.73 (Re_{loc.r})^{0.25} (Re_T)^{0.32} Sc^{0.33} \quad (22)$$

where the nominal and turbulent Reynolds numbers (Re and Re_T) were the local flow variables and defined as $[d_b(u^2+v^2)0.5/\nu]$ and $(d_p u'/\nu)$, respectively. Here, it can be recognized that mass transfer rate depends on the predicted turbulence fluctuation according to :

$$Sh \propto u'^{0.32} \quad (23)$$

Therefore, though mass transfer characteristics are not dealt with in the present study, the effect of the averaged turbulence kinetic energy, which depends on the gas injection flow rate (Fig. 7) and on the inlet areas (Fig. 10), on the mass transfer rate should be allowed for in the design and analysis of a wide variety of materials and chemical processing operations.

5. Conclusion

A numerical model using the Eulerian approach has been used to predict the transport processes in a gas injection system. The calculated results agree well with the experimental results. The turbulent dispersion of the phases within the system has been modeled by the dispersion Prandtl number.

In the present calculation, the bubble size is constant, but this is not the limitation of this model. If information for nonuniform bubble size is available, it can be easily considered in the calculation of the interphase exchange coefficients.

An interesting feature of present work is that the interphase exchange coefficient is calculated with the bubble Reynolds number.

The plume region area and the axial velocities are increased with the gas flow rate and with the decrease in the inlet area. The turbulence growth shows the same trend.

The specific numerical value for the dispersion Prandtl number used in the present calculations may not be applicable to all gas injection systems. Further research needs to be carried out for the prescription of the dispersion Prandtl number. Also, optimal selection for the drag coefficient correlation is needed for other related problems.

For any quantitative predictions in gas injection systems, the present model is expected to provide useful information regarding the two -phase flow. The present study may provide valuable design guidelines and operating limits for new or existing systems.

References

Clift, R. and Grace, J. R. and Weber, M. E., 1978, *Bubbles, Drops, and Particles*, Academic Press Inc., pp. 111~112.

Cross, M., Marcatos, N. C. and Aldham, C., 1984, *Control '84 Mineral Metallurgical Processing*, John A. Herbst, ed., Society of Mining Eng. of the AM. Inst. of Mining, Metallurgical and Petroleum Eng. Inc., New York, NY, pp. 291

~297.

Davidson, J. F. and Schüler, 1960, *Trans. Inst. Chem. Eng.*, Vol. 38, pp. 385~342.

Debroy, T., Majumdar, A. K. and Spalding, D. B., Sept. 1978, *App. Math. Modeling*, Vol. 2, pp. 146~150.

Grevet, J. H., Szekely, J. and El-Kaddah, N., 1982, "An Experimental and Theoretical Study of Gas Bubble Driven Circulation Systems," *Int. J. Heat Transfer*, Vol. 25, No. 4. pp. 487~497.

Johansen, S. T. and Boysan, F., 1988, "Fluid Dynamics in Bubbled Stirred Ladles, Part Ⅱ: Mathematical Modeling," *Metall. Trans. B*, Vol. 19B, pp. 755~764.

Johansen, S. T., Robertson, D. G. C., Woje, K. and Engh, T. A., 1988, "Fluid Dynamics in Bubble Stirred Ladles, Part Ⅰ: Experiments," *Metall. Trans. B*, Vol. 19B, pp. 745~754.

Koh, P. L. T., Markatos, N. C. and Cross, M., 1987, *PCH, PhisicoChem. Hydrodyn.*, Vol. 9(1/2), pp. 197~207.

Mazumdar, D. and Guthrie, R. I. L., 1994, "An Assessment of a Two-Phase Calculation Procedure for Hydrodynamic Modeling of Submerged Gas Injection in Ladles," *ISIJ Int.*, Vol. 34, No. 5, pp. 384~392.

Mazumdar, D. and Guthrie, R. I. L., 1985, "Hydrodynamic Modeling of Some Gas Injection Procedures in Ladle Metallurgy Operations," *Metall. Trans. B*, Vol. 16B, pp. 83~90.

Mazumdar, D., Kajani, S. K. and Ghosh, A., 1990, Steel res., Vol. 61, p. 339.

Mazumdar, D., Verma, V. and Kumar, N., 1992, *Ironmaking Steelmaking*. Vol. 19, p. 152

Mckelliget, J. W., Cross, M. and Gibson, R. D., 1982, *Appl. Math. Mod.*, Vol. 6, pp. 469~480.

Neifer, M., Rodi, S. and Sucker, D., 1993, Investigations on the Fluid Dynamic and Thermal Process Control in Ladles, Steel Res., Vol. 64, pp. 54~62

Oinglin, He, Yichuan, Pen and Tsc-Chiang, Hsiao, Sept. 1984, *Proceedings of Shenyang Symposium of Injection Metallurgy*, IMS, Shenyang, People's Republic of China, pp. 93~113.

Patankar, S. V. and Spalding, D. B., 1972, *Int. J. Heat Mass Transfer*, 15, p. 1787.

Patankar, S. V., 1980, *Numerical Heat Transfer and Fluid Flow*, Hemisphere, Washington D. C.

Sahai, Y. and Guthrie, R. I. L., 1982, Hydrodynamics of Gas Stirred Melts : part Ⅰ. Gas/Liquid Coupling, *Metall. Trans. B*, Vol. 13B, pp. 193~211.

Szekely, J. and Asai, S., 1975, *Trans. ISIJ*, Vol. 15, p. 271.